# *X-ray observations of medium Z H- and He-like ions with satellites from C-Mod tokamak plasmas*



**Citation:** Rice, J E et al. "X-Ray Observations of Medium Z H- and He-Like Ions with Satellites from C-Mod Tokamak Plasmas." Journal of Physics B: Atomic, Molecular and Optical Physics 48, 14 (May 2015): 144013 © 2015 IOP Publishing

**As Published:** http://dx.doi.org/10.1088/0953-4075/48/14/144013

**Publisher:** IOP Publishing

**Persistent URL:** http://hdl.handle.net/1721.1/111169

**Version:** Author's final manuscript: final author's manuscript post peer review, without publisher's formatting or copy editing

PSFC/JA-14-32

# X-ray Observations of Medium Z H- and He-like Ions with Satellites from C-Mod Tokamak Plasmas

Rice, J.E., Reinke[1], M.L., Ashbourn[2], J.M.A., Gao, C., Bitter[3], M., Delgado-Aparicio[3], L., Hill[3], K., Howard, N.T., Hughes, J.W. and Safronova[4], U.I.

[1]present address: University of York, York, UK
[2]University of Oxford, Oxford, UK
[3]Princeton Plasma Physics Laboratory, Princeton, NJ
[4]University of Nevada Reno, Reno, NV

December, 2014

**Plasma Science and Fusion Center**
**Massachusetts Institute of Technology**
**Cambridge MA 02139 USA**

This work was supported by the U.S. Department of Energy, Grant No.DE-FC02-99ER54512. 

# X-ray Observations of Medium Z H- and He-like Ions with Satellites from C-Mod Tokamak Plasmas

J.E. Rice, M.L. Reinke[†], J.M.A. Ashbourn[‡], C. Gao, M. Bitter[♮]
L. Delgado-Aparicio[♮], K. Hill[♮], N.T. Howard, J.W. Hughes and U.I. Safronova[♭]

*Plasma Science and Fusion Center, MIT, Cambridge, MA, USA*

[†]*current affiliation Dept. of Physics, University of York, York, UK*

[‡]*Mathematical Institute, University of Oxford, Oxford, UK*

[♮]*Princeton Plasma Physics Laboratory, Princeton, NJ, USA*

[♭]*Univerity of Nevada Reno, Reno, NV, USA*

## Abstract

X-ray spectra of H- and He-like ions (and satellites) from argon, calcium and chlorine have been obtained from Alcator C-Mod tokamak plasmas using a high resolution x-ray spectrometer system. For H-like charge states, the $Ly_\alpha$ doublet intensity ratio is found to be slightly greater than 1/2 due to interaction with the $^2S_{1/2}$ fine structure sub-level. Neighbouring satellites with spectator electrons occupying n = 2 through n = 7 have been modelled. The $Ly_\alpha$ doublet ratio scalings with electron density and temperature are shown to be in good agreement with collisional-radiative modelling. For He-like ions, the n = 2 satellite intensities are in good agreement with calculations and can be used as an electron temperature diagnostic. The high n Rydberg series has been resolved up to $1s^2$ - 1s16p, and satellites with spectator electrons up to the n = 12 level have been identified.

## I. Introduction

Improvements in high resolution x-ray spectrometers have allowed the detailed study of spectra from medium Z hydrogen-like [1, 2, 3, 4, 5, 6, 7, 8, 9, 10, 11, 12, 13, 14, 15] and helium-like [16, 17, 18, 19, 20, 4, 21, 22, 23, 24, 7, 25, 26, 27, 28, 29, 30, 31, 32, 33, 34, 35, 36, 37, 38, 14, 39, 15] ions in high temperature plasmas. This is made possible by corresponding advances in atomic structure codes, which enables individual line identifications to be made. Collisional-radiative (CR) modelling of line intensities then allows for interpretation of the observed spectra. Since emission line intensities are functions of plasma parameters (such as the density of electrons, impurities or neutrals, and temperatures of electrons or ions) through the various population mechanisms of the upper levels, diagnostic applications are possible. The use of line intensity ratios avoids the necessity of instrument sensitivity calibration and can preclude information on individual charge state densities. In hydrogen-like ions, the emissivity ratio of the $Ly_\alpha$ doublet ($1s\ ^1S_{1/2}$ - $2p\ ^2P_{1/2}$ to $1s\ ^1S_{1/2}$ - $2p\ ^2P_{3/2}$) is a function of electron density at fixed temperature [40, 41, 42, 43, 44]. In helium-like ions, the emissivity ratio of the dielectronic satellite k ($1s^2 2p\ ^2P_{1/2}$ - $1s2p^2\ ^2D_{3/2}$) to the resonance line w ($1s^2\ ^1S_0$ - $1s2p\ ^1P_1$) is only a function of the electron temperature [45], in fact nearly proportional to $1/T_e$ (provided the population of w by radiative recombination of hydrogen-like ions can be ignored). In tokamak plasmas, good independent measurements of the electron temperature and density have allowed for benchmarking of CR modelling codes, such that observed x-ray spectra can be used for determination of the density and temperature when other diagnostics are not available, for example in astrophysical or high energy density plasmas. Furthermore, confidence in modelling of atomic processes in magnetic fusion plasmas allows for spectroscopic measurements to be used to characterize impurity transport, which is an important issue for future reactors.

In this paper, x-ray spectra of H- and He-like ions from argon, calcium and chlorine, including neighbouring satellite lines, are presented after a brief summary of modelling codes and the experimental setup is described in Section II. Section III is devoted to 1s-2p transitions in H-like $Ar^{17+}$ and $Ca^{19+}$, including nearby satellites. The $Ly_\alpha$ doublet intensity ratio is then compared with modeling over a range of electron density and temperature. Observations of the Rydberg series in the He-like ions $Ar^{16+}$, $Ca^{18+}$ and $Cl^{15+}$, including high n satellites and modelling, are presented in Section IV.

## II. Description of Modelling and Experimental Tools

To extract useful plasma diagnostic information from high energy resolution x-ray observations, individual emission line identifications must be made first. This requires accurate calculations of energy levels from atomic structure codes [46, 47, 48, 49]. The next ingredient involves calculations of individual line intensities, which requires accurate wave function determination [50, 51, 18, 52, 53, 54, 55, 56, 57], followed by CR modelling [58, 45, 59, 18]. CR modelling for n = 2 levels in He-like ions follows the methodology in [59]. For n = 2 and n = 3 dielectronic satellites, wavelengths and line factors have been taken from [57] to simulate the observed satellite spectra. Inner shell

excitation rates for n = 2 satellites in $Ca^{18+}$ are from [18]. Wavelengths and line factors for n = 2 and n = 3 dielectronic satellites are also available from [50, 51, 52, 53, 55, 56]. For the higher n Rydberg series and associated satellites in He-like ions, wavelengths and line factors are from the MZ atomic structure code [49, 60, 32]. For the n = 2 levels in H-like ions, CR modelling from the COLRAD code [61, 43, 44] has been used, which includes the effects of electron and ion collisions in the fine structure sub-levels. Wavelengths and line factors for the n = 2 and n = 3 [57], n = 2-7 [56], and n = 5-8 [54] dielectronic satellites have been used to model the satellite spectra.

This study of H- and He-like x-ray spectra has been performed on the Alcator C-Mod tokamak [62], a compact (major radius R $\sim$ 0.67 m, minor radius a $\sim$ 0.21 m, typical elongation of 1.6), high magnetic field (B $\leq$ 8 T) device which has molybdenum plasma-facing components. C-Mod has access to the following confinement regimes: Ohmic and ion cyclotron range of frequencies heated low confinement mode (L-mode), I-mode [63], and enhanced $D_\alpha$ (EDA) [64] and ELM-free high confinement mode (H-mode). Electron densities for this study, determined by Thomson scattering [65], were in the range from $3\times10^{19}/m^3$ to $5\times10^{20}/m^3$ with central electron temperatures (from Thomson scattering and electron cyclotron emission [65]) between 0.8 and 5.5 keV. X-ray spectra were recorded by two separate high energy resolution instruments: a compact, wavelength scanable von Hamos type spectrometer [66] with a quartz 10$\bar{1}$1 crystal (2d = 6.687 Å) and a high resolution, spatially imaging Johann-type spectrometer system [67, 68, 69]. The dispersive element of the Johann spectrometer was a quartz 201 crystal with a 2d spacing of 3.95914 Å. Spectral resolution of the Johann spectrometer system is $\lambda/\Delta\lambda \sim 5000$ with time resolution $\sim$ 6 ms. While sufficient spatial coverage and resolution exist to allow chord-averaged data to be used to determine local emissivities, the results presented here utilize line-averaged spectra. Argon (Z = 18) was puffed into the torus through a piezo-electric valve and chlorine (Z = 17) was introduced by freon ($C_2Cl_3F_3$) injection utilizing a fast scanning probe [70]. Trace amounts of calcium (Z = 20) were introduced into the plasma edge *via* $CaF_2$ injections from a multi-pulse laser blow-off system [71].

### III. Observed H-like Spectra, Satellites and Modelling

This section will examine the 1s-2p spectra of H-like ions and nearby satellites. Shown in Fig.1 is an x-ray spectrum of the H-like $Ar^{17+}$ $Ly_\alpha$ doublet and satellites [4, 6, 13] obtained from a deuterium L-mode discharge with an average electron density $<n_e>$ = $0.7\times10^{20}/m^3$ and a central electron temperature $T_{e0}$ = 2230 eV. This spectrum is dominated by the $Ly_\alpha$ doublet (1s $^1S_{1/2}$ - 2p $^2P_{3/2}$ at 3731.10 mÅ and 1s $^1S_{1/2}$ - 2p $^2P_{1/2}$ at 3736.52 mÅ). Also apparent are several n = 2 dielectronic satellite lines, the brightest of which are J (1s2p $^1P_1$ - 2p$^2$ $^1D_2$ at 3771.79 mÅ) and T (1s2s $^1S_0$ - 2s2p $^1P_1$ at 3755.26 mÅ). Contaminating this spectrum is the 4D transition in $Mo^{32+}$ at 3739.8 mÅ [72] and an unidentified molybdenum line at 3750.4 mÅ. The observed ratio $Ly_{\alpha2}/Ly_{\alpha1}$ is clearly larger than the ratio of the statistical weights of the upper levels, 1/2, and for this case is 0.524$\pm$0.006. This deviation from 1/2 has been attributed to electron and ion collisions in fine structure sub-levels [40, 41, 42]. Shown

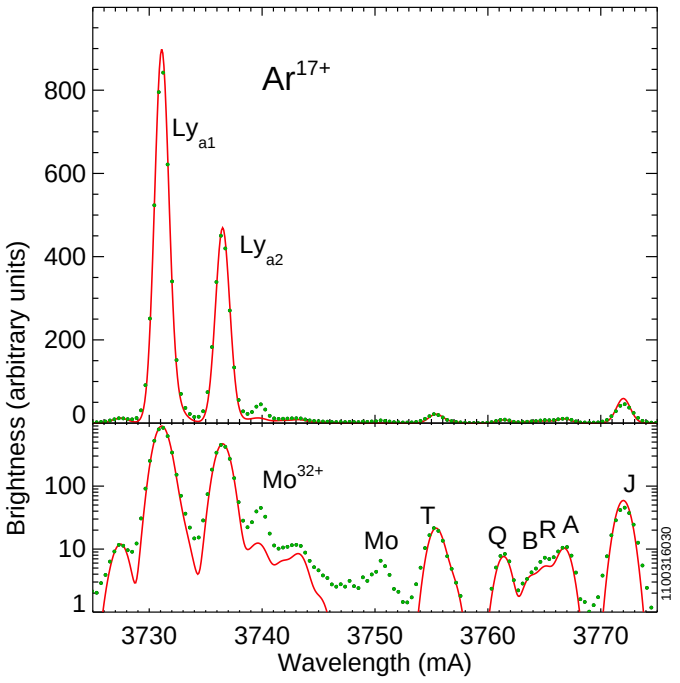


Figure 1: X-ray spectrum of the H-like $Ar^{17+}$ $Ly_\alpha$ doublet and nearby satellites (dots), along with a synthetic spectrum (solid line).

by the solid curve is a synthetic spectrum with the Ly$_\alpha$ doublet calculated from the COLRAD code and with satellites including spectator electrons in levels n = 2 through n = 7 calculated from FAC [56]. The agreement is quite good in wavelength and in relative intensity of the lines. In order to use the measured Ly$_\alpha$ doublet ratio as a plasma diagnostic, care must be taken to account for satellites which fall in the same wavelength range. Satellites with the spectator electron in the n = 2 level, the strongest of which are labeled T, Q, B, R, A and J in Fig.1, are well separated in wavelength from the Ly$_\alpha$ doublet. However, satellites from spectators with n $\geq$ 3 appear underneath the doublet, and must be accounted for.

An expanded view of the synthetic spectrum in the range from 3725 to 3745 mÅ, highlighting the higher n satellites in the vicinity of the doublet, is shown in Fig.2. The contribution from these satellites to the Ly$_\alpha$ doublet intensities at this electron temperature is minimal, less than 1% for even the brightest individual line (note that this is on the same scale as in Fig.1). Two of the brightest n = 3 spectator satellites

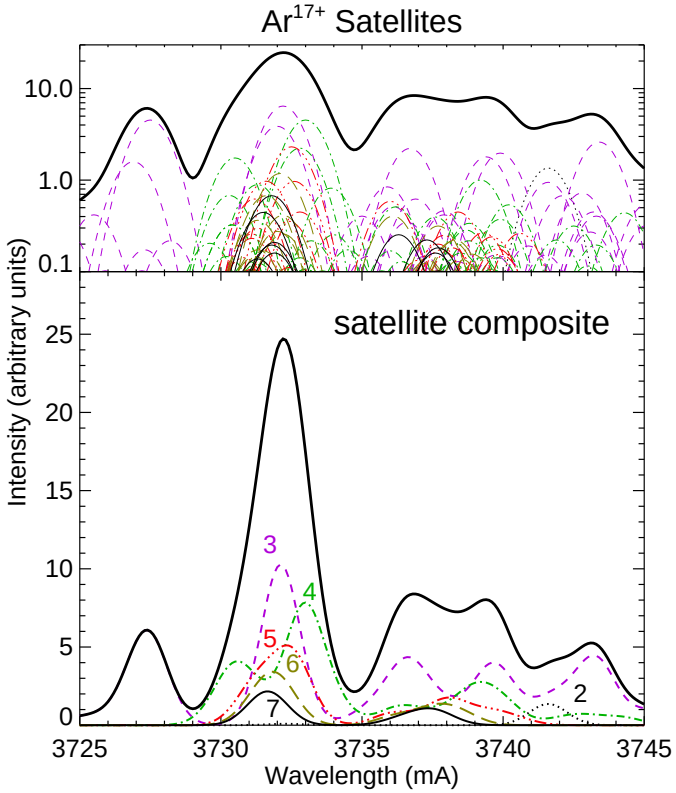


Figure 2: A synthetic spectrum of the satellites to the Ar$^{17+}$ Ly$_\alpha$ doublet, with individual n = 2 (dotted), n = 3 (purple short dash), n = 4 (green dash-dot), n = 5 (red dash-dot-dot-dot), n = 6 (mustard long dash) and n = 7 (solid) satellites (top frame), along with the grand total shown by the thick line. In the bottom frame are shown the satellite composites for each n level, including the combined total.

are 1s3s $^1S_0$ - 2p3s $^1P_1$ at 3732.0 mÅ and 1s3p $^1P_1$ - 2p3p $^1D_2$ at 3732.3 mÅ. In the bottom frame of Fig.2 is shown the composite spectrum for each n level and the total composite of all satellites. The number of individual lines for each n level is: n = 2, 15 lines; n = 3, 51 lines; n = 4, 56 lines; n = 5, 42 lines; n = 6, 30 lines; n = 7, 25 lines. With increasing n, the satellite spectra converge in wavelength and relative intensity to a feature resembling the Ly$_\alpha$ doublet since with high enough n the perturbation to the n = 2 level becomes minimal. Regardless of the electron temperature, the total composite satellite contribution to the Ly$_\alpha$ doublet line ratio is roughly in the same ratio as the Ly$_\alpha$ doublet itself, so has a negligible effect on the inferred ratio.

A similar exercise has been performed for the Ly$_\alpha$ doublet of $Ca^{19+}$, a measured spectrum of which [1, 5, 15] is shown in Fig.3, obtained from a 5.4 T deuterium L-mode discharge with $<n_e>$ = 0.85×10$^{20}$/m$^3$ and $T_{e0}$ = 2800 eV. The measured doublet ratio

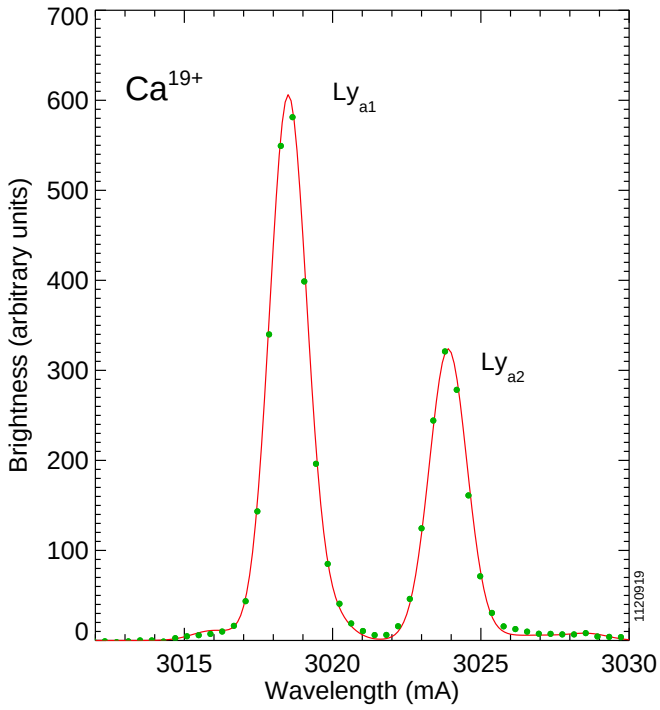


Figure 3: The measured $Ca^{19+}$ Ly$_\alpha$ doublet (dots) and synthetic spectrum (line).

is 0.529±0.003. The synthetic spectrum, which is in excellent agreement, utilized CR modelling for the doublet from COLRAD, for the n = 2 and n = 3 satellites from [57] and for higher n satellites from [54].

The Ly$_\alpha$ doublet ratio has been observed over large electron density and temperature ranges for $Ar^{17+}$ and $Ca^{19+}$. The measured ratios for argon (top) and calcium

(bottom) as a function of electron density are shown in Fig.4 for several operational regimes, unselected for electron temperature. There is little dependence on electron

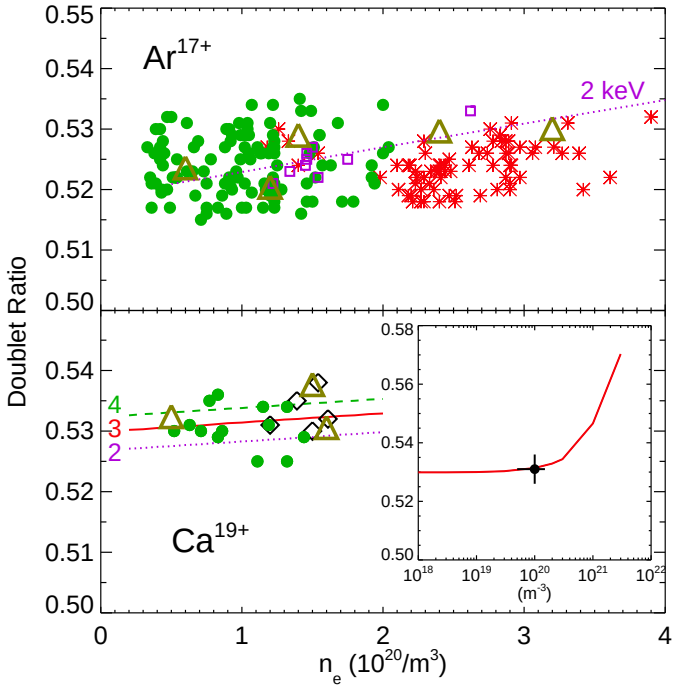


Figure 4: The H-like Ly$_\alpha$ doublet ratio as a function of electron density for $Ar^{17+}$ (top frame) and $Ca^{19+}$ (bottom frame). Dots: L-mode, squares: He plasmas, asterisks: H-mode, diamonds: I-mode and triangles: COLRAD calculations. The dotted line in the top frame is the calculated curve for $T_e$ = 2 keV. The lines in the bottom frame are COLRAD calculations for electron temperatures of 4 keV (dashed), 3 keV (solid) and 2 keV (dotted). The inset in the bottom frame covers a wider density range for $T_e$ = 3 keV.

density (over this range) nor on confinement regime. The average ratio for $Ar^{17+}$ is 0.524$\pm$0.006 and 0.531$\pm$0.005 for $Ca^{19+}$. Shown by the triangles and curves are COLRAD calculations, which are in excellent agreement with observations. In the bottom frame inset, the calcium point is just below the sensitive density region and unfortunately is near the upper limit of tokamak operation. The same ratios as a function of electron temperature are shown in Fig.5, unsorted by electron density. Again, the measured points are in excellent agreement with COLRAD calculations. As can be seen from Figs. 4 and 5, the Ly$_\alpha$ doublet ratio is larger in calcium than in argon. A direct comparison of the ratio as a function of atomic number is shown in Fig.6 for plasmas

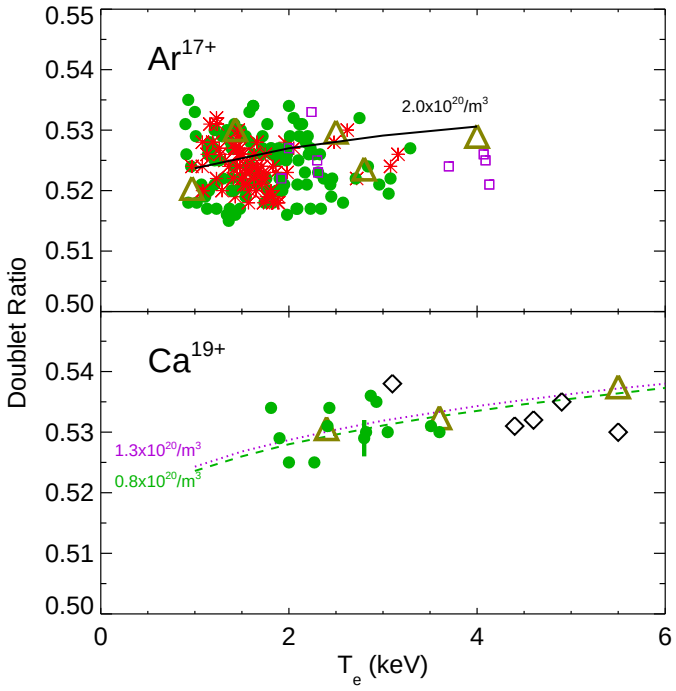


Figure 5: The H-like $Ly_\alpha$ doublet ratio as a function of electron temperature for $Ar^{17+}$ (top frame) and $Ca^{19+}$ (bottom frame). Dots: L-mode, squares: He plasmas, asterisks: H-mode, diamonds: I-mode and triangles: COLRAD calculations. The lines are COLRAD calculations for various electron densities.

with $<n_e>$ = 1.3×$10^{20}$/$m^3$ and $T_{e0}$ = 2.1 keV. COLRAD calculations are depicted by

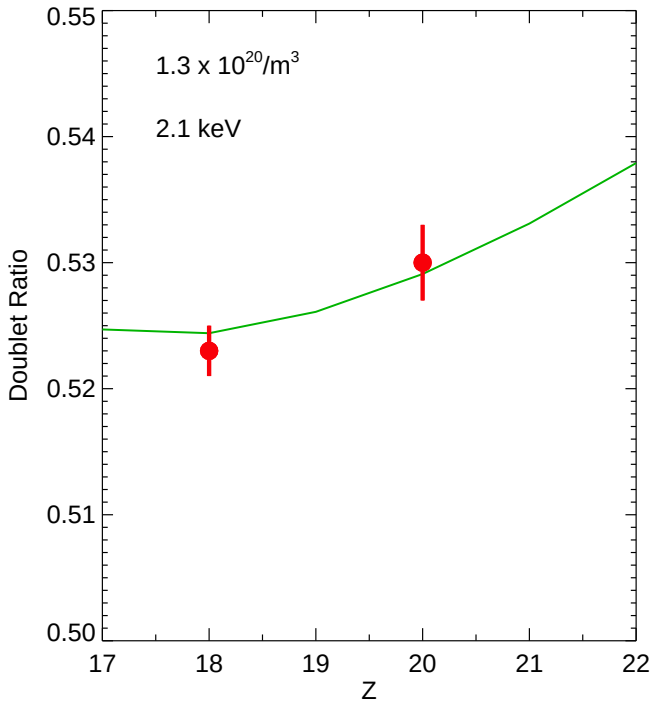


Figure 6: The measured $Ly_\alpha$ doublet ratio as a function of atomic number (dots) for 5.4 T deuterium plasmas with $<n_e>$ = 1.3×$10^{20}$/$m^3$ and $T_{e0}$ = 2.1 keV, along with COLRAD calculations (line).

the curve which is in excellent agreement with the measured points. This ratio difference for different elements is due to a strong Z-dependence of the magnetic dipole transition probability for $2S_{1/2}$ - $1S_{1/2}$ [73, 43, 15].

**IV. Observed He-like Spectra, Satellites and Modelling**

In this section will be discussed x-ray spectra from He-like ions and satellites, including the high n Rydberg series. Presented in Fig.7 is a measured x-ray spectrum of transitions from the n = 2 level in He-like $Ca^{18+}$ and nearby satellites (dots) [18, 30, 34, 35, 15] for a 5.4 T deuterium discharge with $<n_e>$ = 0.6×$10^{20}$/$m^3$ and $T_{e0}$ = 3.5 keV. The resonance (w, $1s^2\ ^1S_0$ - $1s2p\ ^1P_1$, 3177.26 mÅ) and forbidden (z, $1s^2\ ^1S_0$ - $1s2p\ ^3S_1$, 3211.13 mÅ) lines dominate, and intercombination (x, $1s^2\ ^1S_0$ - $1s2p\ ^3P_2$, 3189.19 mÅ and y, $1s^2\ ^1S_0$ - $1s2p\ ^3P_1$, 3192.82 mÅ) lines are prominent,

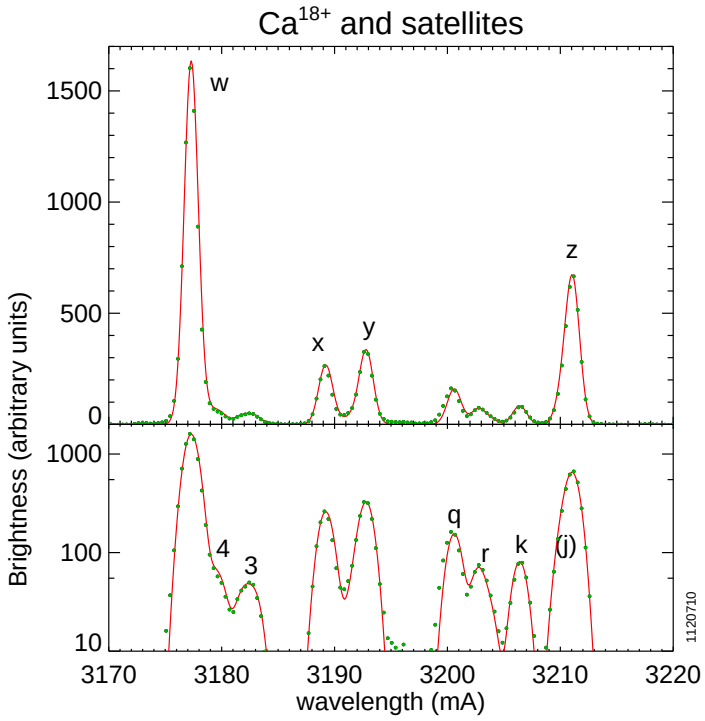


Figure 7: The measured He-like $Ca^{18+}$ (w, x, y and z) spectrum with satellites (most prominent '4', '3', q, r and k) is shown by the dots, with a synthetic spectrum indicated by the solid line.

in addition to n = 2 satellites q, r and k ($1s^2 2p\ ^2P_{1/2}$ - $1s2p^2\ ^2D_{3/2}$, 3206.5 mÅ) and unresolved higher n satellites labelled '3' and '4', with spectator electrons in the n = 3 and n = 4 levels, respectively. The two lines making the strongest contribution to '3' are $1s^2 3p\ ^2P_{1/2}$ - $1s2p3p\ ^2D_{3/2}$ and $1s^2 3p\ ^2P_{3/2}$ - $1s2p3p\ ^2D_{5/2}$. Also shown is a synthetic spectrum, which is in excellent agreement. The He-like transitions were calcualted from the CR model in [59] with theoretical wavelengths from [49]. The n = 2 and n = 3 satellite spectra were generated using wavelengths and line factors from [57], with extrapolations for n = 4.

In the core regions of the plasma where the electron temperature is high, the upper level for w is populated by collisional excitation of the ground state of the He-like ion, while population of the upper level for the satellite k is through dielectronic recombination, also of the He-like ion in the ground state. These two processes have a different dependence on electron temperature, and the ratio of the population mechanisms for k/w scales as $\sim 1/T_e$. This allows the measured line intensity ratio to be used as a temperature diagnostic. Shown in Fig.8 is the measured brightness ratio of k/w in $Ca^{18+}$ as a function of core electron temperature [15] independently determined from Thomson scattering. Also shown is the calculated emissivity ratio from the method which generated the synthetic spectrum of Fig.7, as described above. The agreement is excellent, which gives confidence in the electron temperature diagnostic capability of this ratio when independent temperature measurement is not available. A similar, more rigorous exercise using the tomographically inverted emissivity profiles of $Ar^{16+}$ is also in excellent agreement with modelling [74].

The unresolved satellite group marked '3' in Fig.7 has the spectator electron in the n = 3 level while the n = 2 electron makes the radiative transition. If instead the n = 3 electron makes the radiative transition to the ground state while the n = 2 electron acts as the spectator, the satellite line will appear on the long wavelength side of the $1s^2\ ^1S_0$ - $1s3p\ ^1P_1$ resonance line $w_3$. A similar situation holds for the unresolved satellite group marked '4' with spectators in the n = 4 level; if instead the n = 2 electron acts as the spectator, the corresponding emission line appears as a satellite to the $1s^2\ ^1S_0$ - $1s4p\ ^1P_1$ resonance line $w_4$. An example of this is shown in Fig.9 where the x-ray spectra near $w_2$, $w_3$ and $w_4$ (the first three lines of the Rydberg series) for He-like $Ar^{16+}$ [36] are presented. Several of the individual satellites to the $w_2$ resonance line (top frame) are resolved, in particular q, r and k (see also Fig.7). There is a companion to k, the satellite j ($1s^2 2p\ ^2P_{3/2}$ - $1s2p^2\ ^2D_{5/2}$, 3994.1 mÅ in argon, 3210.2 mÅ in calcium), with a line factor $\sim$1.3 times larger than k, that is unfortunately buried beneath the forbidden line z. The upper levels for these satellites k and j can only be populated by dielectronic recombination of the He-like ionization state. The satellites q and r (and satellites s and t, which are hidden under the intercombination lines x and y) can also be populated be inner shell excitation of the Li-like charge state. The corresponding satellites to the $w_3$ resonance line (middle frame) are unresolved; the strongest satellite groups are labeled $A_3$, $B_3$ and $C_3$. The two strongest contributors to $A_3$ are the transitions $1s^2 2p\ ^2P_{1/2}$ - $1s2p3p\ ^2D_{3/2}$ and $1s^2 2p\ ^2P_{3/2}$ - $1s2p3p\ ^2D_{5/2}$ which are related to k and j, only with the radiating electron initially in the n = 3 level. In a similar fashion $B_3$ is related to q and r, and $C_3$ is related to s and t. Interestingly, the upper levels for the transitions contributing to $A_3$, $B_3$ and $C_3$ are exactly the same as the upper levels for the lines comprising the unresolved satellite group '3' near $w_2$. These are doubly

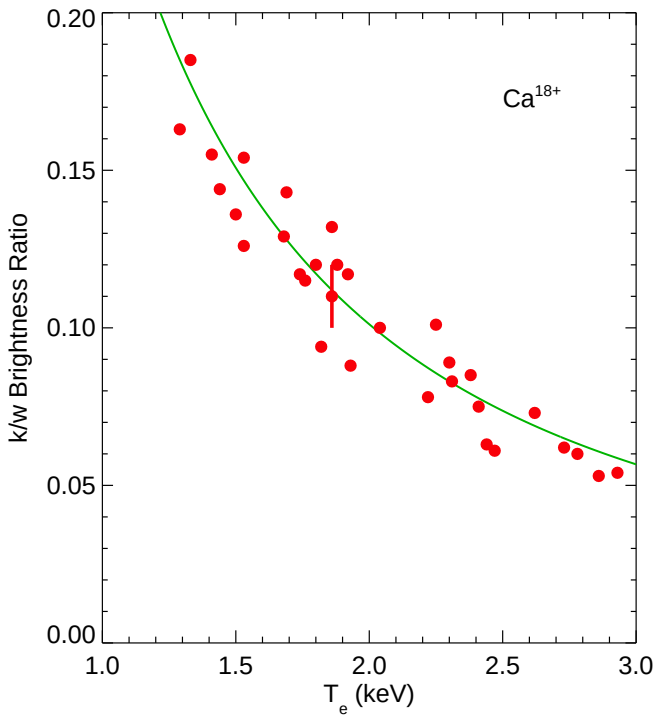


Figure 8: The measured central chord brightness ratio of the dielectronic satellite k to the resonance line w in He-like $Ca^{18+}$ as a function of the central electron temperature (dots) along with the theoretical curve (roughly proportional to $1/T_e$).

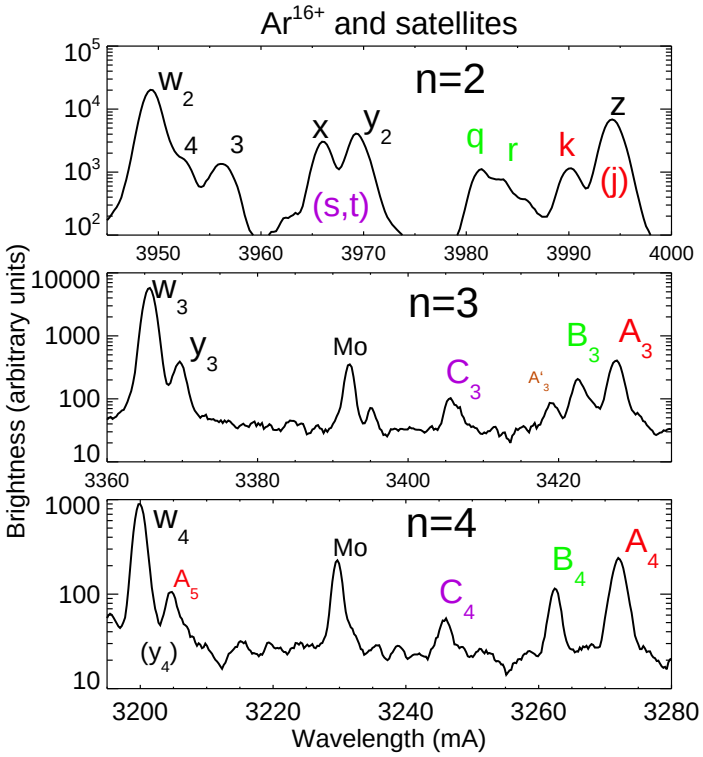


Figure 9: X-ray spectra in the vicinity of the $Ar^{16+}$ resonance lines $w_2$ (top), $w_3$ (middle) and $w_4$ (bottom).

excited states and give rise to either line. Also prominent in the spectrum of the middle frame is the n = 3 intercombination line $y_3$ ($1s^2\ ^1S_0$ - $1s3p\ ^3P_1$); it is much weaker than $y_2$ relative to $w_2$, and closer in wavelength to $w_3$. The corresponding $x_3$ and $z_3$ lines are not visible since they have extremely low transition probabilities. Contaminating this spectrum is the 5D transition in $Mo^{32+}$ at 3392.0 mÅ [72]. A completely analagous situation pertains for the satellites to the resonance line $w_4$ shown in the bottom frame of Fig.9. The three satellite groups $A_4$, $B_4$ and $C_4$ have a very similar pattern to the n = 3 satellite groups; in this case the upper levels for these transitions are the same as those denoted '4' in the top frame. This spectrum is contaminated by the 6D transition in $Mo^{32+}$ at 3230.1 mÅ [72].

An x-ray spectrum in the vicinity of $w_4$, $w_5$ and $w_6$ in the $Ar^{16+}$ Rydberg series is shown in Fig.10, for a discharge with $<n_e>$ = $1.0\times10^{20}/m^3$ and $T_{e0}$ = 1.6 keV. The

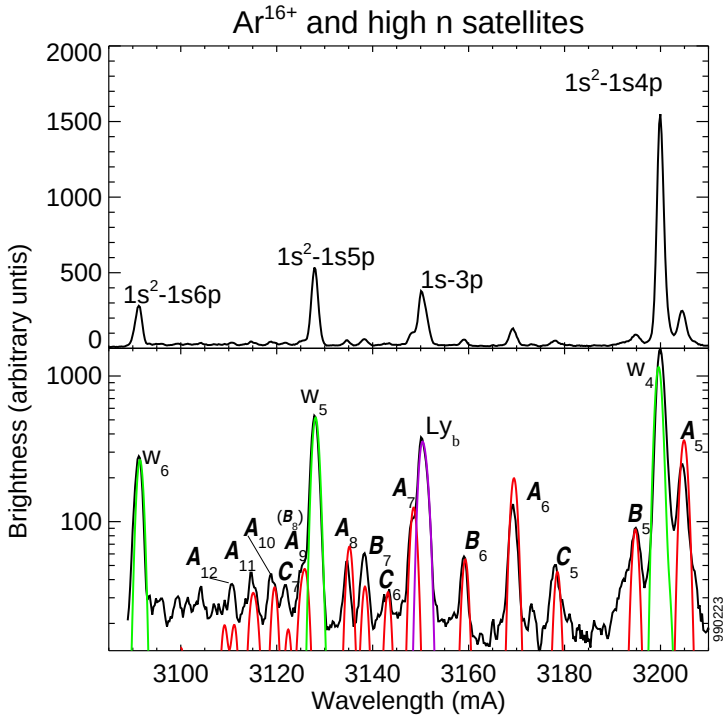


Figure 10: The measured x-ray spectrum of $w_4$, $w_5$ and $w_6$ in $Ar^{16+}$, neighbouring satellites and $Ly_\beta$ in $Ar^{17+}$. In the bottom frame is a synthetic spectrum.

resonance lines fall off in intensity as n increases. The (unresolved) H-like $Ar^{17+}$ $Ly_\beta$ doublet ($1s\ ^1S_{1/2}$ - $3p\ ^2P_{3/2}$, 3150.24 mÅ and $1s\ ^1S_{1/2}$ - $3p\ ^2P_{1/2}$, 3151.38 mÅ) is prominent in the middle of the spectrum. Also apparent are higher n satellite groups. Examination of the log scale spectrum in the bottom frame reveals the satellite groups

$A_5$, $B_5$ and $C_5$, as well as $A_6$, $B_6$ and $C_6$, showing the familiar pattern as in Fig.9. Although the various satellite groups overlap and are crowded together, comparison to the synthetic spectrum in the bottom frame suggests that satellite groups up to $A_{12}$ are identified [32]. This synthetic spectrum of the satellite groups $A_n$, $B_n$ and $C_n$ uses the calculated wavelengths and line factors from the MZ code. Proper line identification relies on the calculated wavelengths, and the observed wavelengths of the high n satellite groups are in excellent agreement with calculations from MZ [32] as demonstrated in Fig.11. This includes observations from $Cl^{14+}$ and $Ar^{15+}$.

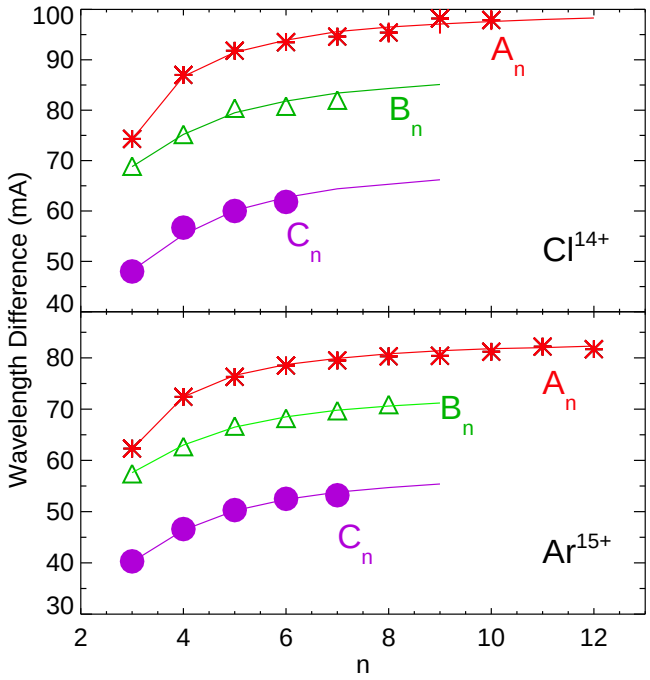


Figure 11: The measured wavelength difference between the resonance lines $w_n$ and the high n satellites groups $A_n$ (asterisks), $B_n$ (triangles) and $C_n$ (dots) for $Cl^{14+}$ ions (top) and $Ar^{15+}$ ions (bottom) as a function of principal quantum number n. Shown by the curves are calculations from the MZ code.

As mentioned above, the $y_3$ intercombination line was identified in the middle frame of Fig.9. There is some evidence for the $y_4$ intercombination line on the long wavelength side of $w_4$, as presented in Fig.12, which shows an expanded view of the region around $w_4$. The synthetic spectrum includes $w_4$ (solid line), the satellite group $A_5$ (dashed line) and two satellites to the H-like $Ar^{17+}$ Ly$_\beta$ doublet (1s2s $^1S_0$ - 2p3s $^1P_1$ at 3197.7 mÅ and 1s2p $^1P_1$ - 2p3p $^1D_2$ at 3206.6 mÅ, dotted lines). These two satellites

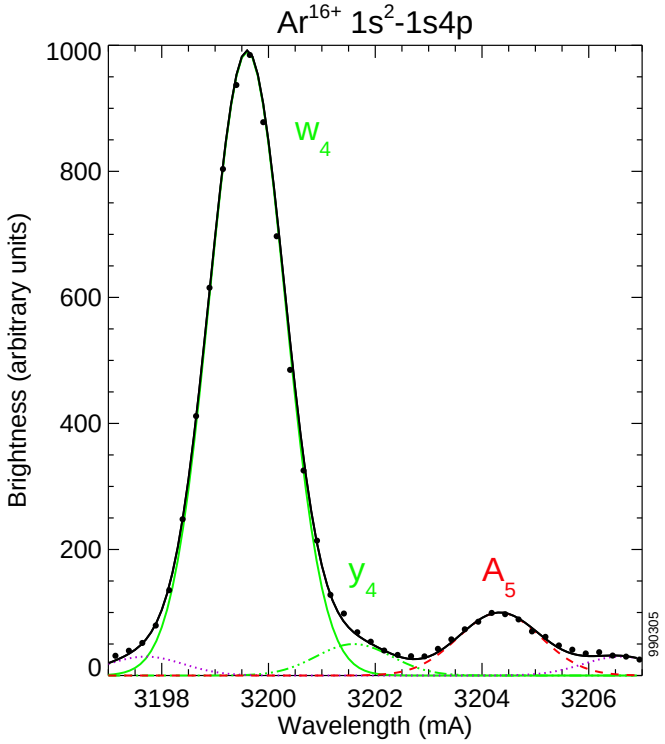


Figure 12: The observed x-ray spectrum near the $w_4$ resonance line in $Ar^{16+}$ is shown by the dots, along with a synthetic spectrum which includes the $A_5$ satellite group (dashed line), the intercombination line $y_4$ (chain line) and two H-like satellites (dotted lines).

to the H-like $Ar^{17+}$ $Ly_\beta$ doublet have the same upper levels as the two strong n = 3 spectator satellites to the $Ly_\alpha$ doublet as shown in Fig.2 and mentioned earlier. Shown by the chain curve is the intercombination line $y_4$, which is in good agreement the observed points. Without inclusion of $y_4$ there would be an excess centred at 3201.5 mÅ. The observed wavelengths for the $y_n$ intercombination lines are in excellent agreement with calculations from the MZ code, as is demonstrated in Fig.13. It is not possible to

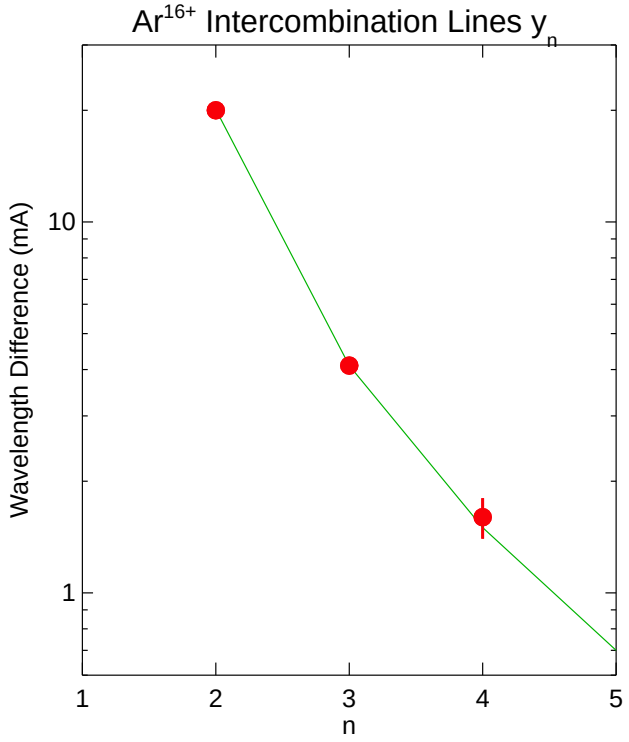


Figure 13: The measured wavelength differences between the resonance lines $w_n$ and intercombination lines $y_n$ as a function of principal quantum number n (dots) compared to MZ code calculations (line).

resolve $y_5$ from $w_5$ experimentally.

For completeness, the $Ar^{16+}$ Rydberg series has been observed near the ionization limit at 3008.79 mÅ and is shown in Fig.14, from a discharge with $<n_e>$ = $0.8\times10^{20}/m^3$ and $T_{e0}$ = 2.6 keV. The resonance lines from $w_6$ to $w_{14}$ are clearly resolved. Also prominent in this spectrum is the unresolved $Ar^{17+}$ $Ly_\gamma$ doublet ($1s\ ^1S_{1/2}$ - $4p\ ^2P_{3/2}$, 2987.34 mÅ and $1s\ ^1S_{1/2}$ - $4p\ ^2P_{1/2}$, 2987.77 mÅ). The continuum radiation between 2990 and 3005 mÅ is noticeably higher than the level seen between the $w_6$ and $w_9$ lines, and is due to radiative recombination.

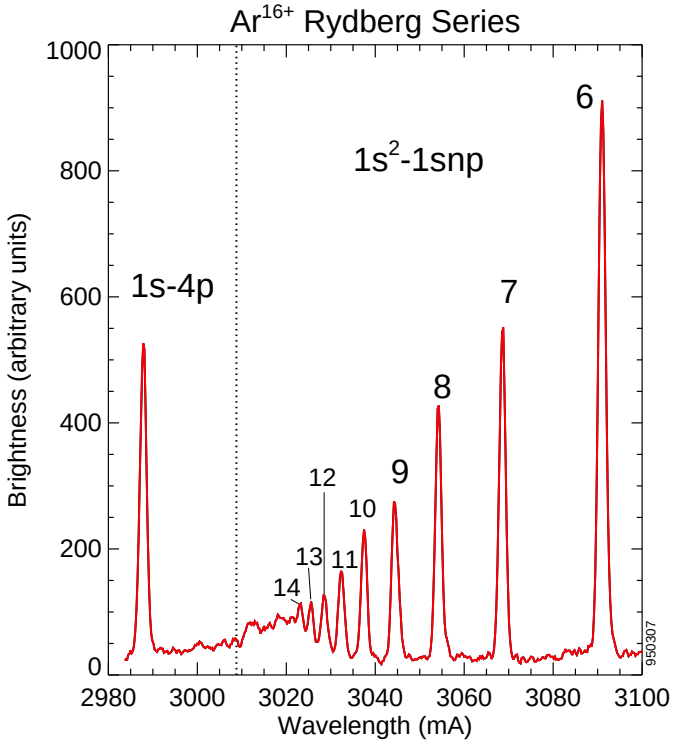


Figure 14: The observed $Ar^{16+}$ Rydberg series between $w_6$ and the ionization limit at 3008.79 mÅ (dotted vertical line), and the unresolved $Ar^{17+}$ $Ly_\gamma$ doublet.

### V. Summary

Observed x-ray spectra in the vicinity of the $Ly_\alpha$ doublet in $Ar^{17+}$ and $Ca^{19+}$, which includes satellites with spectator electrons in levels from n = 2 to n = 7, have been accurately described with collsional-radiative modelling tools for both transition wavelengths and line intensities. The measured $Ly_\alpha$ doublet intensity ratio, which is found to be slightly greater than 1/2, is in good agreement with COLRAD calculations, over a significant range of electron density and temperature, demonstrating its diagnostic capability. For He-like ions there is also good agreement between measured and calculated transition wavelengths and line intensities, for $Ar^{16+}$, $Ca^{18+}$ and $Cl^{15+}$. The brightness ratio between the dielectronic satellite k and the resonance line $w_2$ is in excellent agreement with modelling, and can be used as an electron temperature diagnostic. The high n Rydberg series in $Ar^{16+}$ (up to the ionization limit) and $Cl^{15+}$, and high n satellites (up to n = 12) are in excellent agreement with calculations from the MZ code.

### VI. Acknowledgements

The authors would like to thank M. Chilenski, K. Fournier, M. Gu, A. Hubbard, A. Ince-Cushman, B. LaBombard, Y. Podpaly, S. Wolfe and the Alcator C-Mod operations and ICRF groups for expert running of the tokamak. Work at MIT was supported by DoE Contract No. DE-FC02-99ER54512 and in part by an appointment to the US DoE Fusion Energy Postdoctoral Research Program administered by ORISE.

## References

[1] G.A. Doschek *et al* 1979 *Ap. J.* **233** L157

[2] M. Bitter *et al* 1984 *Phys. Rev. A* **29** 661

[3] E. Källne *et al* 1984 *J. Phys. B* **17** L115

[4] E. Källne *et al* 1985 *Phys. Scr.* **31** 551

[5] L. Blanchet *et al* 1985 *Astron. Astrophys.* **152** 417

[6] E.S. Marmar *et al* 1986 *Phys. Rev. A* **33** 774

[7] F. Bombarda *et al* 1988 *Phys. Rev. A* **37** 504

[8] R. Bartiromo *et al* 1989 *Phys. Rev. A* **40** 7387

[9] H. Kubo *et al* 1992 *Phys. Rev. A* **46** 7877

[10] J.M.A. Ashbourn, I.M. Melnick and N.J. Peacock 2002 *Phys. Rev. E* **65** 066410

[11] J.M.A. Ashbourn, P. McGinnity and N.J. Peacock 2005 *Phys. Rev. E* **71** 017401

[12] H. Bruhns *et al* 2007 *Phys. Rev. Lett.* **99** 113001

[13] J.E. Rice *et al* 2011 *J. Phys. B* **44** 165702

[14] M.F. Gu *et al* 2012 *Can. J. Phys.* **90** 351

[15] J.E. Rice *et al* 2014 *J. Phys. B* **47** 075701

[16] M. Bitter *et al* 1979 *Phys. Rev. Lett.* **43** 129

[17] E. Källne *et al* 1982 *Phys. Rev. Lett.* **49** 330

[18] F. Bely-Dubau *et al* 1982 *Mon. Not. R. Astr. Soc.* **201** 1155

[19] F. Bely-Dubau *et el* 1982 *Phys. Rev. A* **26** 3459

[20] E. Källne *et al* 1984 *Phys. Rev. Lett.* **52** 2245

[21] TFR Group *et al* 1985 *Phys. Rev. A* **32** 2374

[22] TFR Group *et al* 1985 *Phys. Rev. A* **32** 3000

[23] J.E. Rice *et al* 1986 *Phys. Rev. Lett.* **56** 50

[24] J.E. Rice *et al* 1987 *Phys. Rev. A* **35** 3033

[25] M. Bitter *et al* 1993 *Phys. Rev. Lett.* **71** 1007

[26] J.E. Rice *et al* 1995 *J. Phys. B* **28** 893

[27] K.L. Wong *et al* 1995 *Phys. Rev. A* **51** 1214

[28] P. Beiersdorfer *et al* 1995 *Phys. Rev. E* **52** 1980

[29] P. Beiersdorfer *et al* 1996 *Phys. Rev. A* **53** 3974

[30] T. Kato *et al* 1998 *Ap. J.* **492** 822

[31] F.B. Rosmej 1998 *Phys. Rev. E* **58** R32

[32] J.E. Rice *et al* 1999 *New J. Phys.* **1** 19

[33] F.B. Rosmej *et al* 1999 *Plasma Phys. Control. Fusion* **41** 191

[34] J.E. Rice *et al* 2000 *Phys. Plasmas* **7** 1825

[35] J.E. Rice *et al* 2007 *Fusion Sci. Technol.* **51** 357

[36] J.E. Rice *et al* 2007 *Fusion Sci. Technol.* **51** 451

[37] M. Bitter *et al* 2008 *Can. J. Phys.* **86** 291

[38] P. Beiersdorfer *et al* 2009 *J. Phys. Conf. Ser.* **163** 012002

[39] J.K. Rudolph *et al* 2013 *Phys. Rev. Lett.* **111** 103002

[40] V.P. Shevelko *et al* 1976 *J. Phys. B* **9** 2859

[41] N.N. Ljepojevic, R.J. Hutcheon and R.W.P. McWhirter 1984 *J. Phys. B* **17** 3057

[42] G.J. Tallents 1984 *J. Phys. B* **17** 3677

[43] J.M.A. Ashbourn and N.N. Ljepojevic 1995 *Phys. Rev. A* **52** 4966

[44] J.M.A. Ashbourn 1999 *Phys. Rev. E* **59** 6198

[45] A.H. Gabriel 1972 *Mon. Not. R. Astr. Soc.* **160** 99

[46] M. Klapisch 1971 *Comput. Phys. Commun.* **2** 239

[47] G.W. Erickson 1977 *J. Phys. Chem. Ref. Data* **6** 831

[48] M. Klapisch *et al* 1977 *J. Opt. Soc. Am.* **67** 148

[49] L.A. Vainshtein and U. I. Safronova 1985 *Physica Scripta* **31** 519

[50] L.A. Vainshtein and U.I. Safronova 1978 *At. Data Nucl. Data Tables* **21** 49

[51] L.A. Vainshtein and U.I. Safronova 1980 *At. Data Nucl. Data Tables* **25** 317

[52] M.H. Chen 1986 *At. Data Nucl. Data Tables* **34** 301

[53] J. Nilsen 1988 *At. Data Nucl. Data Tables* **38** 339

[54] K.R. Karim *et al* 1996 *J. Quant. Spectrosc. Radiat. Transfer* **55** 431

[55] T. Kato *et al* 1997 *At. Data Nucl. Data Tables* **67** 225

[56] M.F. Gu 2003 *Astrophys. J.* **582** 1241

[57] F.F. Goryayev *et al* 2006 arXiv:physics/0603164v2 [physics.atom-ph]

[58] R. Mewe 1972 *Astron. Astrophys.* **20** 215

[59] R. Mewe and J. Schrijver 1978 *Astron. Astrophys.* **65** 99

[60] U.I. Safronova and J. Nilsen 1994 *J. Quant. Spectrosc. Radiat. Transfer* **51** 853

[61] N.N. Ljepojevic, R.J. Hutcheon and J. Payne 1987 *Comput. Phys. Commun.* **44** 157

[62] E.S. Marmar *et al* 2007 *Fusion Sci. Technol.* **51** 261

[63] D.G. Whyte *et al* 2010 *Nucl. Fusion* **50** 105005

[64] M. Greenwald *et al.* 1997 *Nucl. Fusion* **37** 793

[65] N.P. Basse *et al* 2007 *Fusion Sci. Technol.* **51** 476

[66] J.E. Rice *et al.* 1990 *Rev. Sci. Instrum.* **61** 2753

[67] M. Bitter *et al* 1995 *Rev. Sci. Instrum.* **66** 530

[68] A. Ince-Cushman *et al* 2008 *Rev. Sci. Instrum.* **79** 10E302

[69] M.L. Reinke *et al* 2012 *Rev. Sci. Instrum.* **83** 113504

[70] B. LaBombard *et al* 1999 *J. Nucl. Mater.* **266-269** 571

[71] N.T. Howard *et al* 2011 *Rev. Sci. Instrum.* **82** 033512

[72] J.E. Rice *et al* 1995 *Phys. Rev. A* **51** 3551

[73] N.N. Ljepojevic, R.W.P. McWhirter and S. Volonté 1985 *J. Phys. B* **18** 3285

[74] A. Rosen *et al* 2014 *J. Phys. B* **47** 105701